A Current-Sourced LED Driver Compatible With Fluorescent Lamp Ballasts

Jaeyoung Choi, *Member, IEEE*, Hee-Seok Han, and Kwyro Lee, *Fellow, IEEE*

***Abstract*—A light-emitting diode (LED) driver compatible with fluorescent lamp (FL) ballasts is presented for a lamp-only replacement without rewiring the existing lamp fixture. Ballasts have a common function to regulate the lamp current, despite widely different circuit topologies. In this paper, magnetic and electronic ballasts are modeled as nonideal current sources and a current-sourced boost converter, which is derived from the duality, is adopted for the power conversion from ballasts. A rectifier circuit with capacitor filaments is proposed to interface the converter with the four-wire output of the ballast. A digital controller emulates the high-voltage discharge of the FL and operates adaptively with various ballasts. A prototype 20- W LED driver for retrofitting T8 36-W FL is evaluated with both magnetic and electronic ballasts. In addition to wide compatibility, accurate regulation of the LED current within 0.6% error and high driver efficiency over 89.7% are obtained.**

***Index Terms*—AC/DC conversion, current-sourced converter, duality, fluorescent lamp (FL) ballast, light-emitting diode (LED) driver.**

I. Introduction

THE dramatic depletion of natural resources is giving rise to the ever-increasing cost of energy [1]. Now consumers start looking for energy-efficient solutions with a higher price tag, because they eventually come to less expenditure in the long term. The replacement of the traditional light sources by light-emitting diodes (LEDs) is a perfect example of such a trend. Recent advances in solid-state lighting technologies have shown epoch-making luminous efficacies, which are higher than 150 lm/W [2]. Long life expectancy and environmental safety are other advantages that make the LED promising to be the next generation light source.

The worldwide phase-out of incandescent bulbs has assisted LEDs to make a successful entry into the bulb application [3–5]. In contrast, retrofit LED lamps for fluorescent lamps (FLs) are still struggling to get attention from consumers. The difference arises from the fact that FLs require a dedicated device called "ballast." In an FL fixture, the ballast is installed in between an FL and the ac main supply, as depicted in Fig. 1(a). A forthright scheme is to replace both ballast and FL with an ac line LED driver and an LED lamp, as shown in Fig. 1(b) [6–10]. Another possible scheme is to replace only the FL with a ballast-compatible LED lamp, which includes a converter to operate at the ballast output, as shown in Fig. 1(c) [11], [12]. Despite the lower luminous efficacy due to the loss of the ballast, the compatible solution is still competitive because it is not only convenient but also safe. Therefore, more recently, lamp manufacturers have introduced ballast-compatible LED lamps even though they already have ac-line powered LED products [13], [14]. Several LED drivers have been published as well. In [11], a passive LED driver based on the phasor transformation theory was proposed, but it is compatible only with rapid-start magnetic ballasts. A phase-shift resonant converter demonstrated its compatibility with both magnetic and electronic ballasts in [12]. Nevertheless, the converter circuit is complicated with many magnetic components.

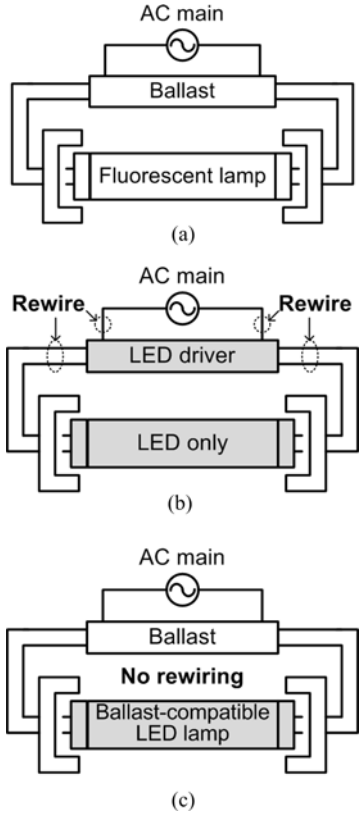

Fig. 1. Installation of different lamps in the FL fixture. (a) FL. (b) LED lamp with a separate ac-line LED driver. (c) LED lamp compatible with the ballast.

Manuscript received April 10, 2014; revised July 10, 2014; accepted August 16, 2014. Date of publication August 27, 2014; date of current version March 5, 2015. This work was supported by the National Research Foundation of Korea grant funded by the Korea government (MEST) (No. 2010-0015119) and by HiDeep Inc., Korea. Recommended for publication by Associate Editor J. M. Alonso.

J. Choi is with the Institute of Microelectronics, A*STAR, Singapore, 117685 (e-mail: choijy0623@gmail.com).

H.-S. Han is with Silicon Mitus Technology, Cupertino, CA 95014 USA (e-mail: heeseok.han@gmail.com).

K. Lee is with the Department of Electrical Engineering, Korea Advanced Institute of Science and Technology, Daejeon 305-701, Korea (e-mail: krlee@kaist.ac.kr).

Digital Object Identifier 10.1109/TPEL.2014.2352462

To design an LED driver compatible with ballasts, we start with the observation that FL ballasts can be modeled as non-ideal current sources. The power drawn from ballasts can be controlled by loading a converter whose input is assumed to be a current source. A rectifier circuit with frequency-dependent filaments offers a full compatibility with both magnetic and electronic ballasts. In addition, a digital feedback controller is designed for adaptive operations with widely different ballast topologies. As a result, high efficiency and accurate current regulation are verified with various commercial ballasts.

II. Review and Modeling of FL Ballasts

The FL is one of the most widely used gas-discharge lamps, especially in offices and industrial workspaces. Gas-discharge lamps are electrically open before they are turned ON. To turn ON the lamp, a high voltage needs to be applied across filament electrodes. After the lamp is turned ON, it exhibits a negative-resistance characteristic due to impact ionization [15]. Therefore, a voltage source such as the ac main supply cannot drive the FL directly and a ballast should be introduced between the lamp and the voltage source. Ballasts can be categorized into two groups: magnetic ballast and electronic ballast.

A. Magnetic Ballast

The magnetic ballast is literally made up of a large magnetic coil on the order of a few henries. The large inductance stabilizes the lamp current despite the decrease in the lamp impedance. In other words, the ac main supply and the inductor build an ac current source together. The operating frequency is identical to the frequency of the ac main supply $f_{\rm AC}$, which can be either 50 or 60 Hz.

Magnetic ballasts can be classified further by their connection with lamps. In a lamp fixture with a glow-start magnetic ballast, a starter is used in parallel with the lamp, as shown in Fig. 2(a) [16]. This type of ballast is merely an inductor, and as discussed previously, the fixture is equivalent to a model shown on the right. The model consists of two paths, ac current path and auxiliary path for the connection with the starter. Another common type is the rapid-start magnetic ballast [17]. This type adopts a transformer, which has additional windings to heat the filaments on its own. A connection diagram of the rapid-start magnetic ballast is shown along with the equivalent model in Fig. 2(b). Again there is main path and auxiliary path, where only the former has to do with the current-source nature. Windings for the filament are modeled as dependent voltage sources v_f.

B. Electronic Ballast

Magnetic ballasts are simple and durable, but they suffer from audible noise and flickering. These nuisances can be eliminated if the FL is operated by the electronic ballast, whose operating frequency is high as several tens of kilohertz. Typically, the electronic ballast consists of two cascaded converters. A power factor correction (PFC) circuit produces a dc voltage source from the ac main supply. Both passive and active circuits are widely adopted for the PFC [18], [19]. Following the PFC circuit is a resonant inverter, which generates a high frequency from the PFC output. Half-bridge or push–pull inverters are used and each of them can be either current fed or voltage fed [20], [21]. Despite their various topologies, all electronic ballasts utilize parallel resonant networks. The parallel resonant inverter behaves like a current source if it is operated at the resonant frequency [22]. Actually, the output current of the electronic ballast decreases slowly with increase in the load resistance. This is because the switching frequency of the inverter is chosen to be slightly higher than the resonant frequency for the zero-voltage switching [23]. But after the lamp is lit, the quality factor becomes lower and the ballast can be regarded as a current source.

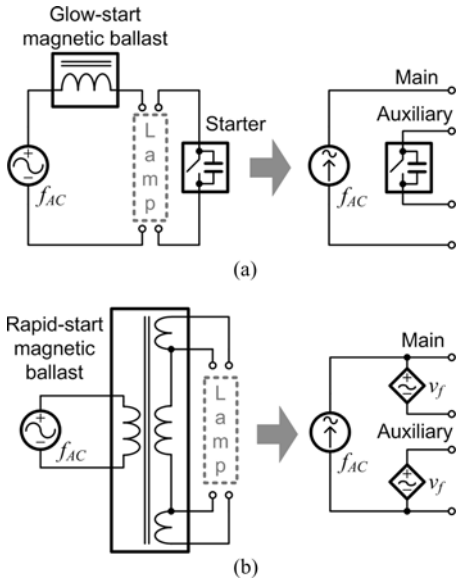

Fig. 2. Magnetic ballasts and equivalent models. (a) Glow-start magnetic ballast with a starter switch. (b) Rapid-start magnetic ballast based on a transformer to heat filaments.

Two popular architectures of electronic ballasts are illustrated here. A simplified circuit of an instant-start current-fed half-bridge ballast is shown in Fig. 3(a). The PFC circuit is simplified to a dc voltage source $V_{\rm PFC}$. Transformer and capacitor C_p make the parallel resonant circuit. An equivalent model can be constructed by substituting the resonant inverter including voltage-limiting capacitor C_b by an ac current source. The ac frequency generated by the inverter is denoted by $f_{\rm carrier}$. The other common type is the rapid-start voltage-fed half-bridge ballast, whose simplified circuit and equivalent model are shown together in Fig. 3(b). A half-bridge inverter is directly fed by $V_{\rm PFC}$, and a parallel resonant circuit is formed by C_p and inductor L. The ballast can be modeled as a current source, which has four output terminals. It is important to note that the current-source characteristic is maintained only when all four terminals are in operation, which is different from the case of magnetic ballasts where two of the terminals form a current source.

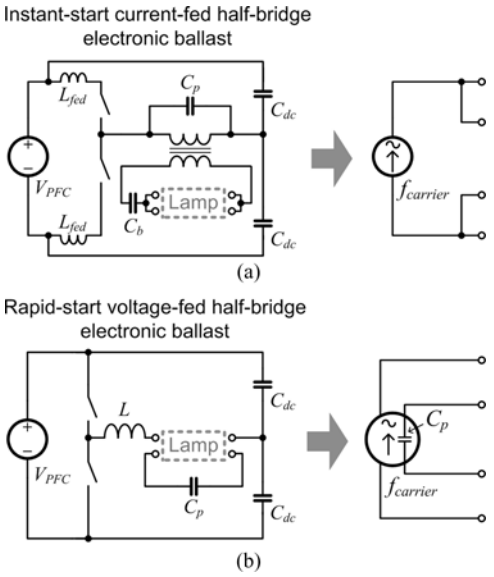

Fig. 3. Two of the most common electronic ballasts and equivalent models. (a) Instant-start current-fed half-bridge electronic ballast. (b) Rapid-start voltage-fed half-bridge electronic ballast.

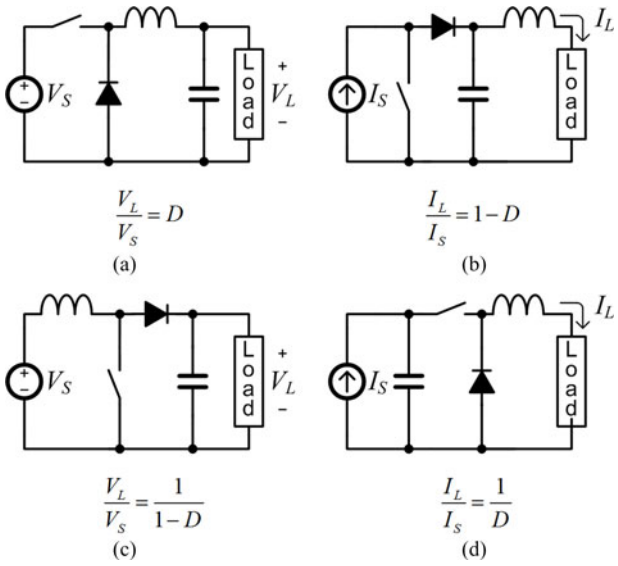

Fig. 5. Dual converters and their conversion ratios. (a) Voltage-sourced buck. (b) Current-sourced buck. (c) Voltage-sourced boost. (d) Current-sourced boost.

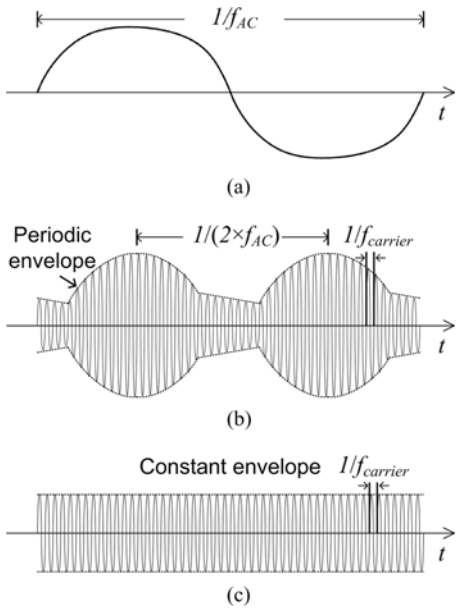

Fig. 4. Output current waveforms of various ballasts. (a) Magnetic ballast (b) electronic ballast with a valley-fill PFC (c) electronic ballast with a boost PFC.

C. Output Current Waveforms in the Steady State

As ballasts differ widely in circuit topology, output current waveforms also vary considerably. Magnetic ballasts operate at $f_{\rm AC}$, and some harmonic components may appear as shown in Fig. 4(a). Electronic ballasts generate amplitude-modulated signals whose $f_{\rm carrier}$ is as high as tens of kilohertz. The envelope is determined by the PFC circuit in the ballast. If a passive PFC such as the valley-fill PFC is employed, the envelope changes slowly with a period of $1/(2 \times f_{\rm AC})$ as the waveform given in Fig. 4(b). On the other hand, if an active PFC such as the boost PFC is employed, the envelope does not change as shown in Fig. 4(c). In summary, the periodicity differs significantly with different ballasts. Moreover, $f_{\rm AC}$ differs from region to region as 50 or 60 Hz. This is one of the main challenges in implementing a ballast-compatible LED driver.

III. Current-Sourced Converter for the Ballast-Compatible LED Lamp

Voltage sources, such as the ac main supply and batteries, can be found almost everywhere in our daily lives. Therefore, general power converters tacitly assume their input to be voltage sources [24]. These converters are referred to as voltage-sourced (VS) converters in this paper. In a VS converter, a desired output power is obtained by drawing a controlled current from a fixed input voltage. This principle is not applicable when the input is a current source whose output current cannot be changed. For the current-sourced (CS) situation, a controlled voltage needs to be established for a fixed input current. Converters for the aforementioned function are referred as CS converters, and can be derived from VS counterparts using the duality principle [25].

Dual converters can be constructed by substituting voltage sources to current sources, series connections to parallel connections, inductors to capacitors, closed switch to open switch, and vice versa. Two of the most basic converters, buck and boost converters, are shown with their dual circuits in Fig. 5(a)–(d). The CS converters are governed by the principle of capacitor amp-second balance, whereas VS converters are governed by the principle of inductor volt-second balance. The conversion ratio of the CS boost converter in Fig. 5(d) is calculated here. Source current and load current are denoted as I_S and I_L, respectively. When the switch is OFF, I_S flows into the capacitor. When the switch is ON, $I_L - I_S$ flows out of the capacitor. In the steady state, charge variations during a switching period are

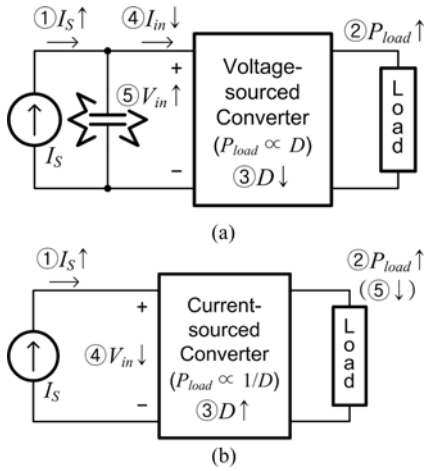

Fig. 6. Responses to I_S increase in VS and CS converters. (a) VS converter fails to regulate $P_{\rm load}$ because it tries to adjust $I_{\rm in}$ (b) CS converter absorbs I_S as it is, and $P_{\rm load}$ is regulated by adjusting $V_{\rm in}$.

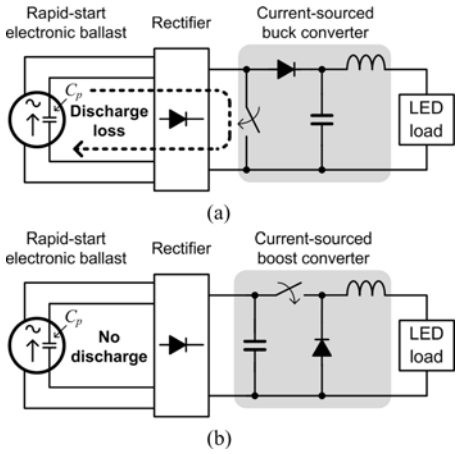

Fig. 7. Operations of CS converters with the rapid-start electronic ballast. (a) C_p discharge loss due to the parallel switching in the buck converter. (b) Shielding effect in the boost converter.

balanced and the conversion ratio I_L/I_S can be derived as

$$I_S t_{\rm off} + (I_S - I_L) t_{\rm on} = 0 \tag{1}$$

$$\frac{I_L}{I_S} = \frac{t_{\rm on} + t_{\rm off}}{t_{\rm on}} = \frac{1}{D} \tag{2}$$

where $t_{\rm off}$ and $t_{\rm on}$ are durations of off- and on-state, respectively, and *D* is the duty cycle. Similarly, I_L/I_S for the CS buck converter in Fig. 5(b) can be derived as (*1–D*). Other topologies of CS converters are described in [26] and [27].

A. Input Current Regulation in VS and CS Converters

The necessity of the CS converter becomes clear when the line regulation behavior is investigated. The critical difference between VS and CS converters is that directions of the *D* control are opposite to each other. This is because the load power $P_{\rm load}$ is proportional to *D* in VS converters, whereas $P_{\rm load}$ is inversely proportional to *D* in CS converters. Suppose a current source I_S is filtered by a capacitor and a VS converter is adopted, as shown in Fig. 6(a). If I_S is increased for some reason, $P_{\rm load}$ increases as a result. The VS converter decreases *D*, expecting the converter input current $I_{\rm in}$ to be decreased. However, this increases imbalance between incoming and outgoing currents of the capacitor and only brings a further increase in the input voltage $V_{\rm in}$. The converter will continue to decrease *D*, and the capacitor will eventually blow up due to the excess voltage.

On the other hand, the CS converter adjusts the input potential $V_{\rm in}$ through which I_S flows. The response of the CS converter to the increase in I_S is illustrated in Fig. 6(b). In response to the increased $P_{\rm load}$, the CS converter increases *D* so that $V_{\rm in}$ is decreased. This process does not conflict with the current source. As a result, the input power into the converter ($I_S \times V_{\rm in}$) returns to the original value and $P_{\rm load}$ remains regulated.

B. Considerations in Choosing a Converter Topology

Nonidealities and application-specific constraints should be carefully considered in choosing a converter topology. The ballast can have a nonzero output conductance and it may result in a significant power loss if a switch-first topology, such as buck or buck–boost converter, is adopted. Suppose the output of the rapid-start electronic ballast is connected to the CS buck converter, as shown in Fig. 7(a). The capacitor C_p is discharged every time the buck switch is closed. The discharging loss can be calculated as

$$\text{Discharing Loss with the CS Buck} = f_{\rm switch} C_p v_{Cp}^2 \tag{3}$$

where $f_{\rm switch}$ is the switching frequency and v_{Cp} is the voltage on C_p, which is close to the LED voltage. If we assume typical values of 5 nF and 40 V for C_p and v_{Cp}, then the loss can be considerable as 1.6 W with 200-kHz switching. On the other hand, as shown in Fig. 7(b), the input of the CS boost converter is a parallel capacitor, which shields the converter from nonidealities of the current source. Therefore, not only the discharging loss is avoided but also the ballast is unaffected by the switching.

The CS boost converter is also preferable when safety regulations for the LED lamp are considered. If the output voltage of an LED driver exceeds dc 60 V, it is considered that a risk of fire or electric shock exists and safety requirements become more stringent [28]. The CS boost converter allows the selection of a low-voltage LED load for the same lamp power.

IV. Four-Input Rectifier Circuit for Improving Compatibility With FL Ballasts

An FL has four terminals and each two terminals are connected by filament electrodes. The LED lamp does not require electrodes because it is not a gas-discharge lamp. Nevertheless, shorting two adjacent terminals induces excess current in the rapid-start magnetic ballast whose transformer windings drive filaments. In addition, shorted filaments may disturb startup processes of program-start ballasts. On the other hand, the rapid-start electronic ballast requires low-impedance filaments to preserve the resonant circuit. Previously, a compatible LED driver implemented the actual impedance of the filament by inductors [29]. However, it is not appropriate for a full compatibility with

both low-frequency and high-frequency ballasts. In this paper, an adaptive rectifier circuit utilizing the difference between magnetic and electronic ballast is proposed. For the case of magnetic ballasts, auxiliary paths are only intended for heating filaments. They have nothing to do with the current-source operation. On the other hand, for the case of the rapid-start electronic ballast, filaments are parts of the resonant network, which is the key for the current-source operation. Therefore, the rectifier is desired to allow filament currents only when it is connected to electronic ballasts.

To implement such a function, capacitive filaments C_f are inserted in parallel to two full-bridge rectifiers. Output of the rectifiers are combined and connected to four types of ballasts in Fig. 8(a)–(d). The frequency-dependent filaments allow current flow only when electronic ballasts are connected, by taking advantage of the thousand-fold difference between operating frequencies. The redundant starter in the glow-start fixture is disabled, as shown in Fig. 8(a). Unnecessary filament currents become negligible with the rapid-start magnetic ballast, as depicted in Fig. 8(b). The instant-start electronic ballast is also not affected by the rectifier, as shown in Fig. 8(c). Finally, the parallel resonant network in the rapid-start electronic ballast is maintained, as shown in Fig. 8(d). The value of C_f is chosen to be sufficiently larger than C_p in the electronic ballast (usually a few nanofarads), to retain the original resonance. The voltage on C_f is nonzero with rapid-start ballasts, and the actual voltage is determined by the voltage division with C_p. The circuit achieves the full compatibility, which enables users to retrofit the LED lamp without identifying the ballast inside the lamp fixture.

V. Design of the Proposed LED Driver

A detailed circuit diagram of the proposed LED driver is presented in Fig. 9. A 20-W LED load whose forward voltage and current are 37 V and 530 mA is chosen to substitute a 36-W T8 FL. The lamp will reuse the preexisting lighting fixture. Four output wires of the ballast are connected to diode bridges $D_1 - D_8$ with frequency-dependent filaments. The output current of the ballast $i_{\rm ballast}$ is rectified and fed to a CS boost converter. A switch controller senses the switch current $i_{\rm SW}$ and determines the duty cycle of the gate signal $v_{\rm gate}$. It also monitors the voltage at the anode of the LED load v_H to manipulate the lamp startup transient. A Schottky diode D_{10} is used in the converter to improve the efficiency. The electrolytic capacitor C_2 is added to suppress the ripple in the LED current $i_{\rm LED}$. The linear FL is much bigger in size than the incandescent bulb, and the driver circuit can be sparsely placed for a heat management. Nevertheless, the temperature inside the package should be carefully examined to avoid the lifetime shortening due to the use of an electrolytic capacitor.

A. Lamp Startup Procedure

Some program-start electronic ballasts detect whether the load is an intact FL. The proposed LED driver emulates the high-voltage discharge of the FL in order not to disturb normal operations of ballasts, as shown in Fig. 10. When the ballast

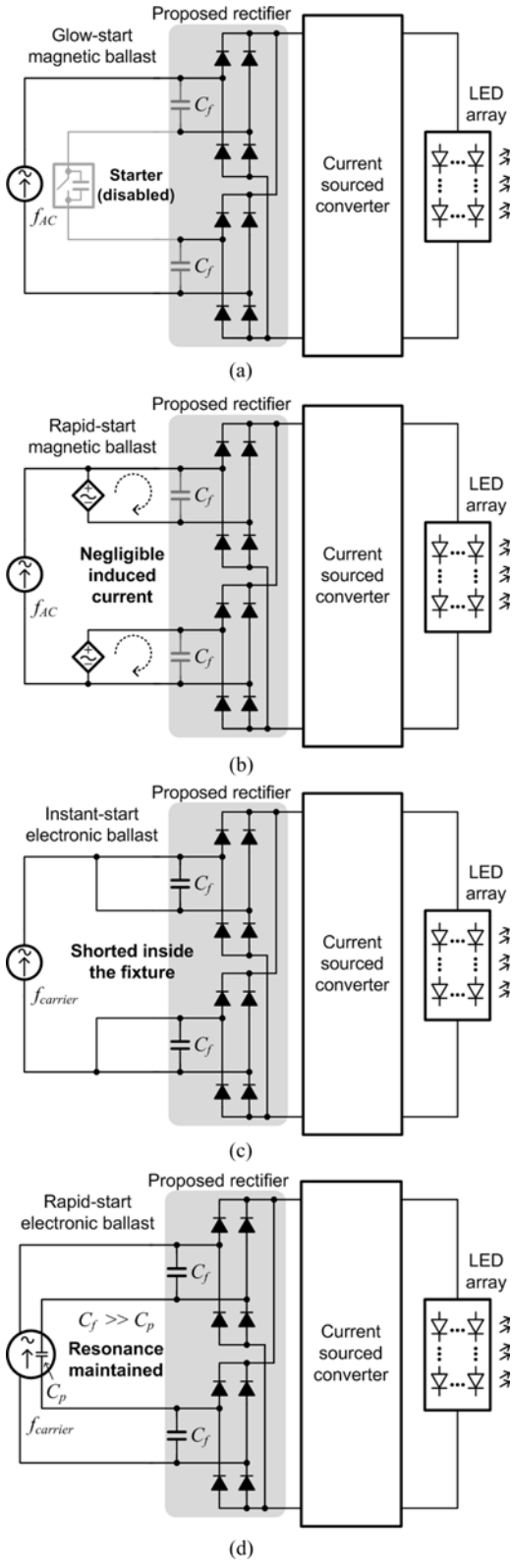

Fig. 8. Proposed rectifier circuit applied to different ballasts. Preheating paths are selectively connected and disconnected according to the type of ballasts. Operation with (a) glow-start magnetic ballast (b) rapid-start magnetic ballast (c) instant-start electronic ballast (d) rapid-start electronic ballast.

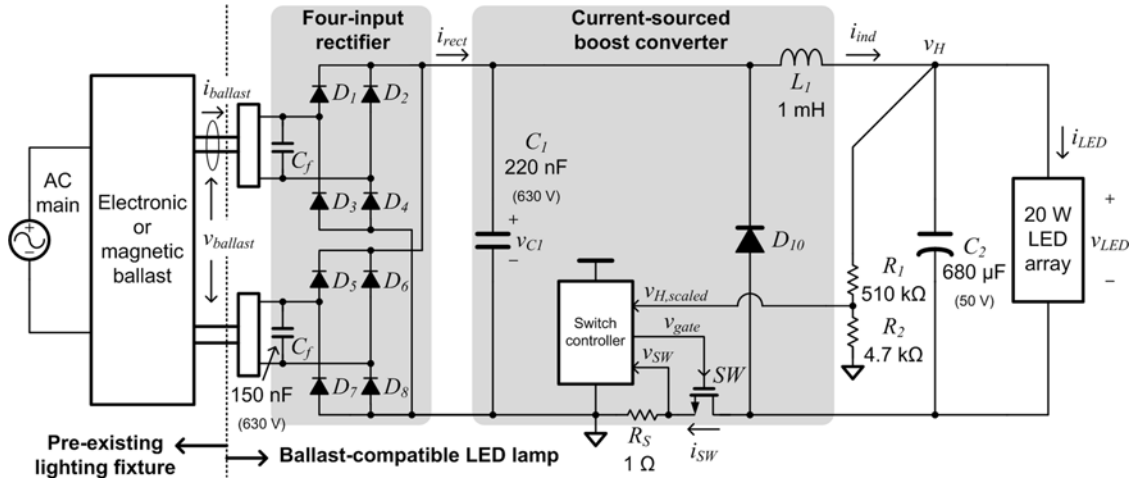

Fig. 9. Circuit diagram of the proposed LED driver shown together with ballast and LED load.

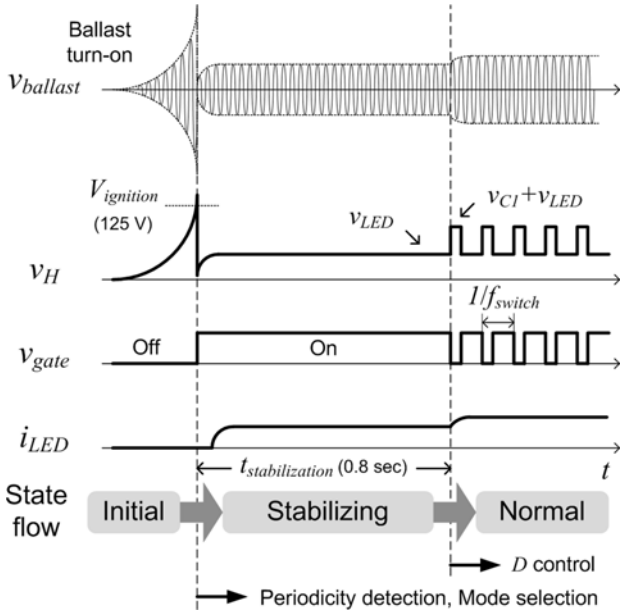

Fig. 10. Emulation of the high-voltage discharge and state transitions of the switch controller.

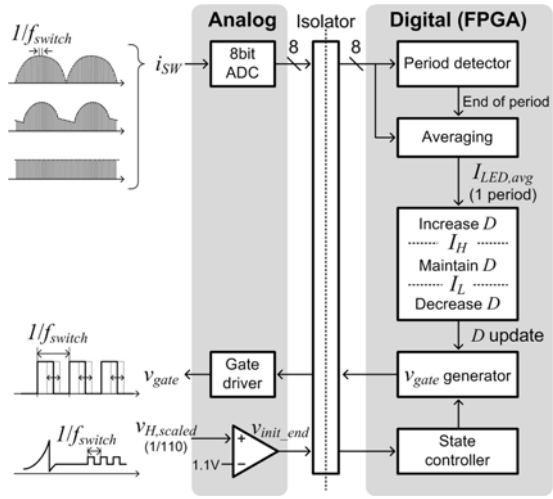

Fig. 11. Block diagram of the switch controller.

is turned ON, the lamp voltage first needs to rise freely until it reaches a threshold voltage for the discharge. This is simply achieved by keeping the boost switch *SW* open, so that the clamping load is disconnected from the ballast. The controller monitors v_H instead of the voltage on $C_1(v_{C1})$, because v_H can be also utilized to sense the voltage across the LED $v_{\rm LED}$ when the switch is closed. At the moment when v_H exceeds a given voltage $V_{\rm ignition}$, the switch is closed and a sudden voltage drop occurs by the charge sharing between C_1 and C_2. The controller waits for a fixed time $t_{\rm stabilization}$ for the ballast to be stabilized, and then, the feedback control of D is enabled. The stabilizing state is also a preparation time for the adaptive controller to identify which type of ballast is used. Values for $V_{\rm ignition}$ and $t_{\rm stabilization}$ are chosen empirically and denoted in Fig. 10.

B. Adaptive Feedback Controller

A block diagram of the switch controller is shown in Fig. 11. Core functions are implemented in the digital domain using a field programmable gate array (FPGA). Digital isolator chips separate the signal ground from the FPGA ground. The high-voltage signal v_H is divided by resistors R_1 and R_2, and a comparator generates a flag signal for the state transition. After the controller enters the normal state, the feedback loop is enabled to regulate the average of the LED current $I_{\rm LED,avg}$. An 8-bit analog to digital converter (ADC) samples $i_{\rm SW}$ during the switch is closed, to obtain the inductor current $i_{\rm ind}$. The sampled $i_{\rm ind}$ is periodically averaged to obtain $I_{\rm LED,avg}$, and the averaging period is determined according to the ballast in use. At the end of each period, $I_{\rm LED,avg}$ is compared with upper and lower limits of the desired LED current I_H and I_L. The controller decreases D if $I_{\rm LED,avg}$ is under the regulation band ($I_{\rm LED,avg} < I_L$), and increases D if $I_{\rm LED,avg}$ is over the regulation band ($I_{\rm LED,avg} > I_H$). In the case when $I_{\rm LED,avg}$ is in the desired band, D is maintained. A digital pulse generator

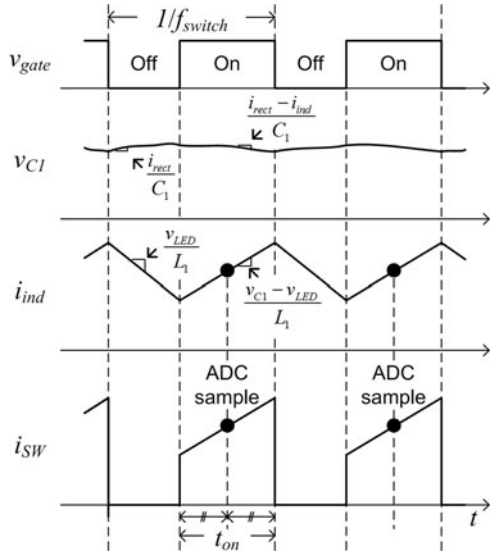

Fig. 12. Key waveforms of the CS boost converter. The ADC samples $i_{\rm ind}$ at the middle of $t_{\rm on}$ to accurately sense the instantaneous average of $i_{\rm ind}$.

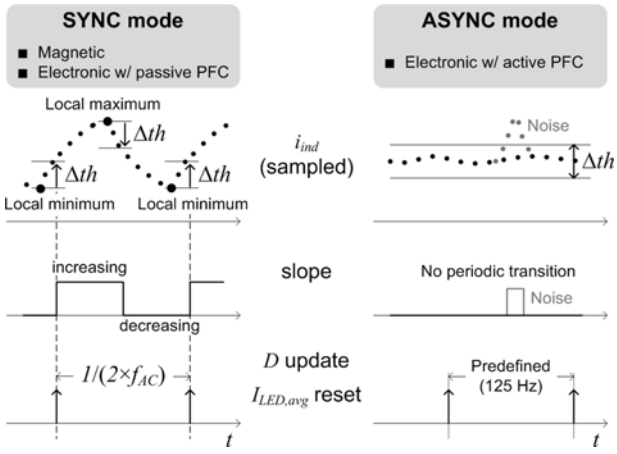

Fig. 13. Two modes of the switch controller. If $i_{\rm ind}$ is periodic, SYNC mode is selected. In the opposite case, ASYNC mode is selected.

produces $v_{\rm gate}$, which has a duty of *D*, and the pulse is buffered by a high-voltage gate driver chip in the analog domain. The analog board is powered by a 12-V adapter and the current consumption is 20 mA.

Waveforms of the capacitor voltage v_{C1}, $i_{\rm ind}$, and $i_{\rm SW}$ are illustrated in Fig. 12, along with $v_{\rm gate}$. The switching frequency is denoted as $f_{\rm switch}$. During $t_{\rm on}$, $i_{\rm ind}$ changes with a slope of

$$\frac{di_{\rm ind}}{dt} = \frac{v_{C1} - v_{\rm LED}}{L_1} \tag{4}$$

where L_1 is the inductance at the converter output. High-frequency components are suppressed sufficiently to make v_{C1} nearly constant within the switching period. Then, $i_{\rm ind}$ changes linearly during $t_{\rm on}$ and the controller can obtain the instantaneous average of $i_{\rm ind}$ by sampling $i_{\rm SW}$ at the middle of $t_{\rm on}$. This scheme requires a continuous conduction in L_1.

A proper choice of passive components removes only high-frequency components, so that the low-frequency envelope remains in $i_{\rm ind}$. If a magnetic ballast or an electronic ballast with the passive PFC is in use, the sampled $i_{\rm ind}$ changes gradually with a frequency of $2 \times f_{\rm AC}$. On the other hand, if an electronic ballast with the active PFC is used, the sampled $i_{\rm ind}$ does not show such a periodicity. To operate adaptively with different periodicities, the proposed controller supports two modes of operation, which are depicted in Fig. 13. While the sampled $i_{\rm ind}$ is averaged, a period detector tracks local minimum and maximum in a period. A valid transition of the slope is recognized when $i_{\rm ind}$ deviates more than a threshold Δth from local extremes. By choosing an appropriate value for Δth, false detections due to the noise can be minimized without affecting the period detection. If the sign of the slope changes regularly, the controller goes into SYNC mode, where the averaging process is restarted at the rising edge of the detected slope. On the other hand, if the slope rarely changes or does not change at all, the controller goes into ASYNC mode. In ASYNC mode, since there is not a periodicity with which the controller can synchronize, a predefined periodic pulse is generated internally. The period for ASYNC mode is chosen as 125 Hz in this study. The mode selection is done repeatedly even after the target $I_{\rm LED,avg}$ is reached. This prevents the controller from operating in a wrong mode permanently owing to transient or startup noise.

C. Design Equations and Component Details

Considerations in choosing values for $f_{\rm switch}$, C_1, L_1, and C_2 are summarized here. First of all, $f_{\rm switch}$ is desired to satisfy

$$f_{\rm switch} - 2 \times f_{\rm carrier} > 20\,{\rm kHz}\ ({\rm highest\ audio\ frequency}) \tag{5}$$

so that audible noise can be prevented. The multiplication by 2 comes from the rectification of the ballast current. A frequency of 200 kHz is chosen for $f_{\rm switch}$ in this study.

The sensing method in the proposed controller requires v_{C1} to be nearly constant within the switching period. A ripple of 5% is allowed in this design and the voltage ripple Δv_{C1} can be calculated as

$$\Delta v_{C1} = \frac{I_{\rm rect,avg} \times t_{\rm off}}{C_1} \le V_{C1,\rm avg} \times 0.05 \tag{6}$$

where $I_{\rm rect,avg}$ and $V_{C1,\rm avg}$ are average values of $i_{\rm rect}$ and v_{C1}, respectively. The proposed LED driver adopts the CS boost converter, where $t_{\rm off}$ and $V_{C1,\rm avg}$ is related to $I_{\rm rect,avg}$ as

$$\frac{I_{\rm rect,avg}}{D} = \frac{1/f_{\rm switch}}{1/f_{\rm switch} - t_{\rm off}} \times I_{\rm rect,avg} = 530\,{\rm mA} \tag{7}$$

$$I_{\rm rect,avg} \times V_{C1,\rm avg} \cong 20\,{\rm W} \tag{8}$$

where 530 mA and 20 W are desired LED current and power. Power losses in the converter are ignored for simplification. If we assume $I_{\rm rect,avg}$ to be 400 mA, $t_{\rm off}$ and $V_{C1,\rm avg}$ in the steady state would be 1.25 μs and 50 V, respectively. Then, C_1 needs to be larger than 200 nF. The value selected in this study is 220 nF.

The output current of the converter $i_{\rm ind}$ is desired to contain only the low-frequency envelope. This is achieved by a proper choice of L_1. A power converter is equivalent to a canonical

TABLE I
LIST OF COMPONENTS USED IN THE PROTOTYPE LED DRIVER

Component	Part No.	Note
$D_1 - D_8, D_9$	FR105	600 V diode
D_{10}	MBRS3201T3G	200 V Schottky diode
SW	IRF830	4.5 A, 500 V, 1.5 Ω N-MOSFET
Gate driver	IR4427	-
Comparators	TS331	Open-drain comparator
ADC	ADS7866	Serial output ADC
Isolators	Si8663	Digital isolator
FPGA	Xilinx Virtex-6	-

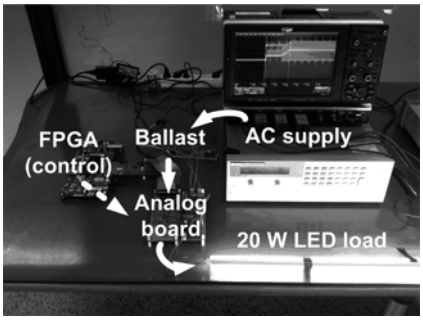

Fig. 14. Measurement setup.

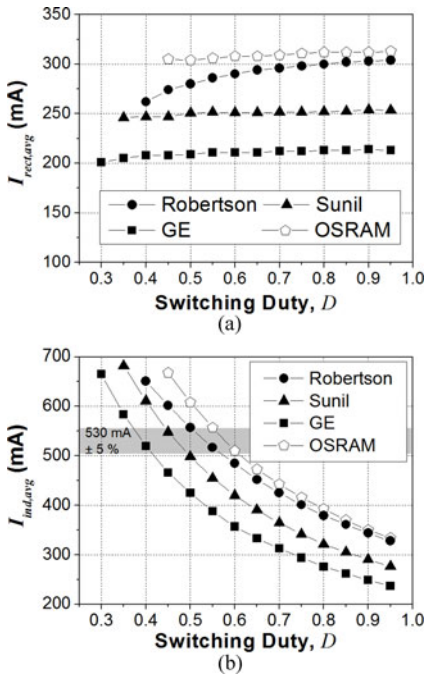

Fig. 15. Open-loop responses of the CS converter with various ballasts. (a) Average of the rectifier output current, which is the converter input. (b) Average of the inductor current, which is the converter output.

circuit model, which contains a second-order low-pass filter [24, p. 253]. In the VS boost converter, the switching action scales the inductor by $1/(1–D)^2$. If the duality principle is applied for the CS boost converter, it is the capacitor at the input, which is scaled by $1/D^2$. Then, the cutoff frequency $f_{\rm cutoff}$ is designed to satisfy

$$2 \times f_{AC} \ll f_{\rm cutoff} = \frac{D}{2\pi\sqrt{L_1 C_1}} \ll 2 \times f_{\rm carrier}. \quad (9)$$

Another consideration in choosing L_1 value is the current rating, which decreases as the inductance increase for a package type. A practical value of 1 mH is chosen considering the desired output current of 530 mA, and $f_{\rm cutoff}$ is placed at ($D \times 11$ kHz).

The role of C_2 is to suppress the low-frequency envelope in $i_{\rm LED}$. A value of 680 μF is chosen through measurements using a number of ballasts. Table I shows details of components used in the prototype lamp. Ratings for capacitors are denoted in Fig. 9.

VI. EXPERIMENTAL VERIFICATION

The prototype LED driver is evaluated with nondimmable 36-W ballasts of various types discussed in previous sections. The list includes rapid-start magnetic ballast Robertson RN320P, rapid-start electronic ballast with a valley-fill PFC Sunil KS-F2321, instant-start electronic ballast GE 23671, and program-start electronic ballast OSRAM QTP8 1×36. A photograph of the measurement setup is given in Fig. 14. An ac supply powers the ballast under test. The ballast is loaded with the proposed ac–dc converter, which in turn drives the LED load. The analog board includes rectifier, converter, and analog-digital interface circuits. The digital controller is implemented by the FPGA. A series of measurements was repeated for each ballast.

A. Open-Loop Responses

The measured $I_{\rm rect,avg}$ is almost constant with *D* regardless of the ballast type, as shown in Fig. 15(a). This confirms the current-source nature of ballasts, and suggests that the CS converter can be a proper choice to implement an LED lamp compatible with ballasts. Meanwhile, the average current at the converter output $I_{\rm ind,avg}$ increases by the boost function of *1/D*. The desired LED current of 530 mA can be reached by different *D* values for different ballasts, as highlighted in Fig. 15(b).

B. Lamp Operation During Startup

The LED lamp starts with the proposed emulation procedure, and all of the ballasts start normally. The startup waveforms of the LED lamp with magnetic ballast, instant-start electronic ballast, and program-start electronic ballast are shown in Fig. 16 (a)–(c), respectively. A slow increase in v_{C1} is observed with the program-start ballast, which is different from immediate impulses with other ballasts. No overshoot in $i_{\rm LED}$ is observed. The LED array turns ON within 0.4 s from the moment when $v_{\rm AC}$ is turned ON, and $i_{\rm LED}$ reaches 95% of the desired value within 1.6 s.

After the stabilization, the switch controller starts to decrease *D* at the end of each period and the output current is increased in the next period. Adaptive operations with magnetic ballast, electronic ballast with a valley-fill PFC and electronic ballast with a boost PFC are shown in Fig. 17(a)–(c), respectively. High-frequency components at $f_{\rm carrier}$ and $f_{\rm switch}$ are

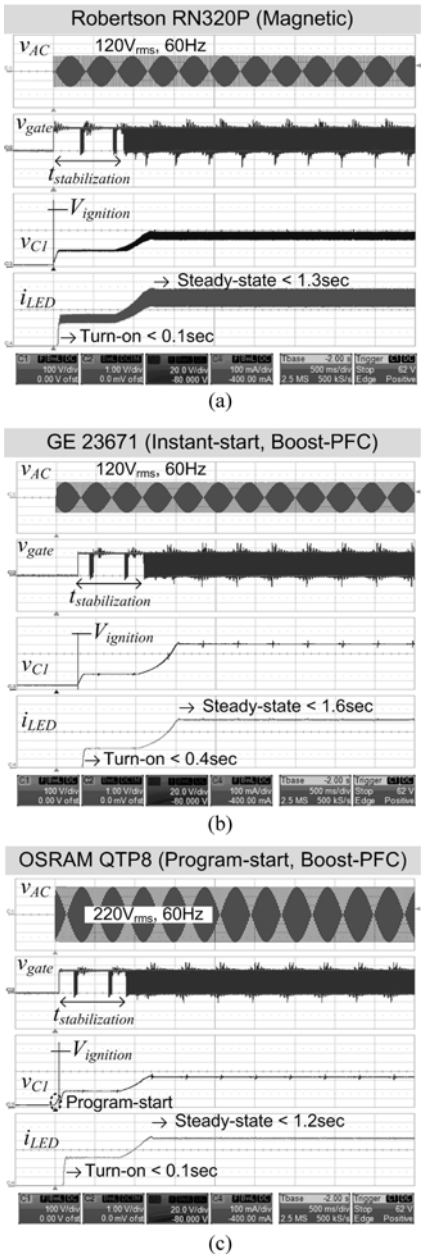

Fig. 16. Lamp startup transient waveforms (Timebase: 500 ms/div, Ch1: 100 V/div, Ch2: 1 V/div, Ch3: 20 V/div, Ch4: 100 mA/div) (a) with a magnetic ballast (b) with an instant-start electronic ballast (c) with a program-start electronic ballast.

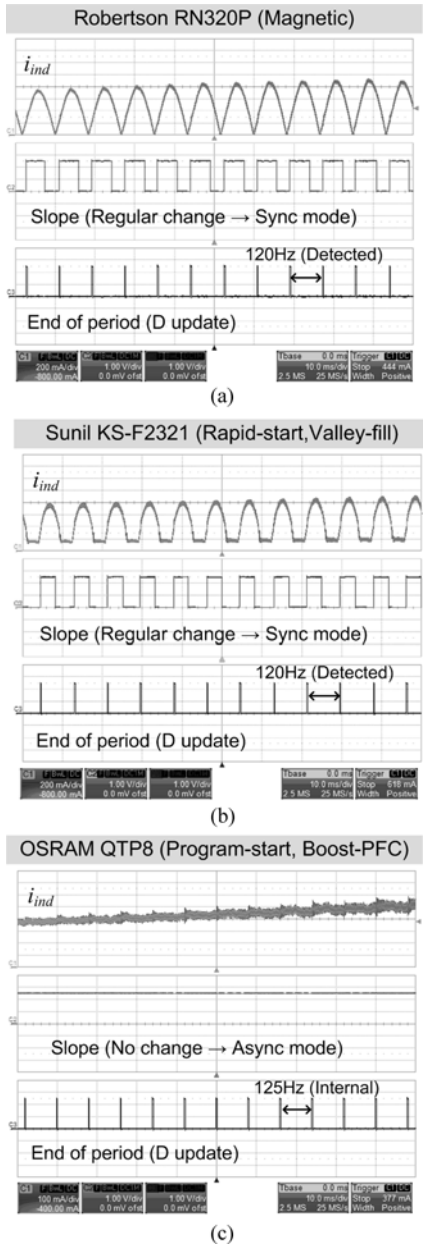

Fig. 17. Adaptive feedback operation by the period detection (Timebase: 10 ms/div, Ch2&Ch3: 1 V/div) (a) with a magnetic ballast (Ch1: 200 mA/div) (b) with an electronic ballast which has a valley-fill PFC (Ch1: 200 mA/div) (c) with an electronic ballast which has a boost PFC (Ch1: 100 mA/div).

suppressed by passive components in the converter and the envelope of the ballast current is dominant in $i_{\rm ind}$. The slope signal shows a good synchronization with various waveforms of $i_{\rm ind}$. The end-of-period flag signal indicates that the controller has selected SYNC mode for periodic-envelope ballasts and ASYNC mode for the constant-envelope ballast.

C. Lamp Operation in the Steady State

Voltage and current waveforms at input and output of the LED driver in the steady state are shown in Fig. 18(a)–(d), for each ballast. It should be noted that the output voltage of the ballast $v_{\rm ballast}$ ranges from 63.6 to 98.6 $V_{\rm rms}$, which is much lower than the typical voltage swing across the 36-W FL ($\approx$140 $V_{\rm rms}$). This means that the LED driver introduces a smaller load resistance at the ballast output, which results in a smaller power drawn from the current source. Different ballasts have different output current levels, but the converter adjusts $v_{\rm C1}$ to regulate the LED current closely. The error from the desired value of 530 mA is only from -0.6% to $+0.2\%$. The low-frequency ripple is mainly suppressed by C_2 and the worst case ripple current is 229 $\rm mA_{pp}$ with the valley-fill electronic ballast.

Switching waveforms of two different electronic ballasts in the steady state are given in Fig. 19(a) and (b). Recall that GE 23671 has the smallest output current and OSRAM QTP8

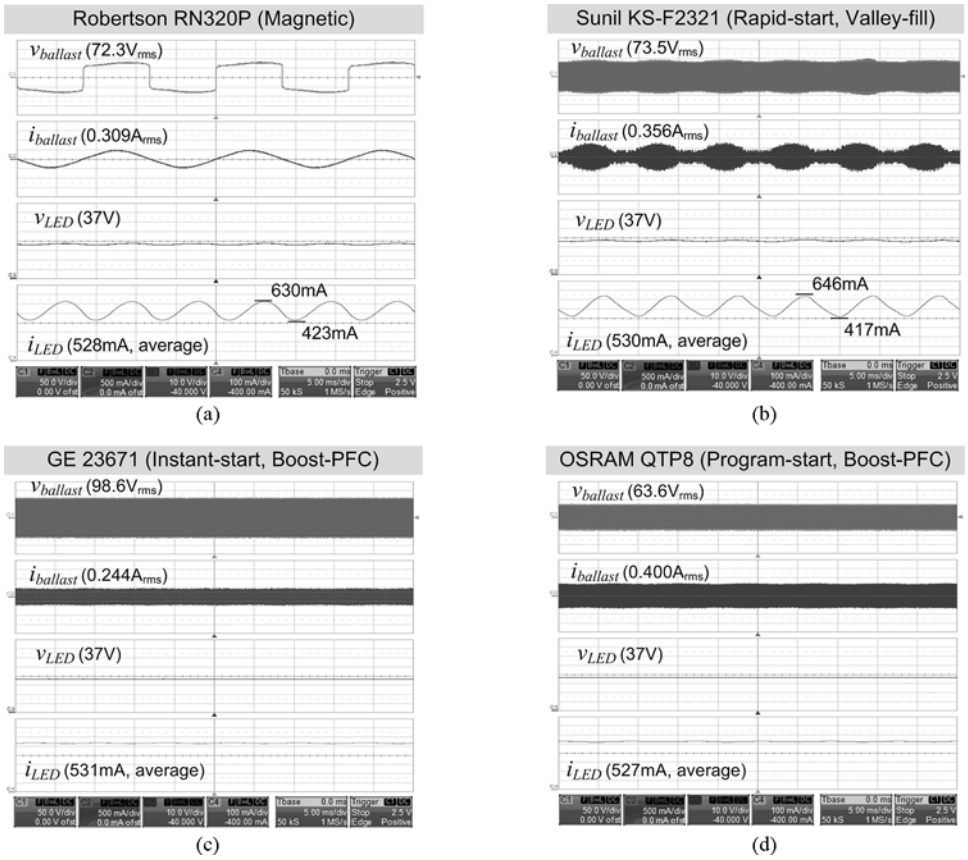

Fig. 18. Steady-state voltage and current waveforms at input and output of the LED driver (Timebase: 5 ms/div, Ch1: 50 V/div, Ch2: 500 mA/div, Ch3: 10 V/div, Ch4: 100 mA/div) (a) with the magnetic ballast Robertson RN320P (b) with the valley-fill PFC electronic ballast Sunil KS-F2321 (c) with the electronic ballast GE 23671 (d) with the electronic ballast OSRAM QTP8 1×36.

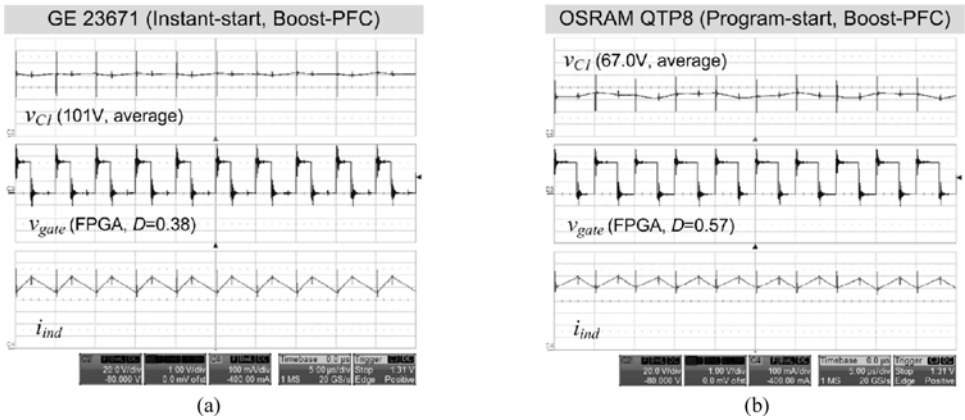

Fig. 19. Switching waveforms in the steady state (Timebase: 5 μs/div, Ch2: 20 V/div, Ch3: 1 V/div, Ch4: 100 mA/div) (a) with the electronic ballast GE 23671 which has a smallest output current (b) with the electronic ballast OSRAM QTP8 1×36, which has the largest output current.

1×36 has the largest output current, as shown in Fig. 15(a). To regulate $I_{\mathrm{LED,avg}}$, steady-state D values are proportional to the input current level and v_{C1} values are inversely proportional to them. For all four ballasts, D ranges from 0.38 to 0.57 and the average of v_{C1} ranges from 67.0 to 101 V.

Power factor (PF) and total harmonic distortion (THD) with the retrofit LED lamp are also measured and compared to those with the FL. The magnetic ballast RN320P is a normal PF ($<$0.9) ballast without a PF correction. Measured PF and THD were 0.63 and 13.7% with the FL, and changed to 0.52 and 5.6% with the LED lamp, respectively. Measured PF and THD of the electronic ballast with a valley-fill PFC were 0.93 and 19.0%, which degraded to 0.91 and 26.8%, respectively. Nevertheless, the ballast still can be classified as a high PF ($>$0.9) ballast. Ballasts with the active PFC were rather insensitive to the load. Measured PF and THD of GE 23671 were 0.99 and 7.6% with

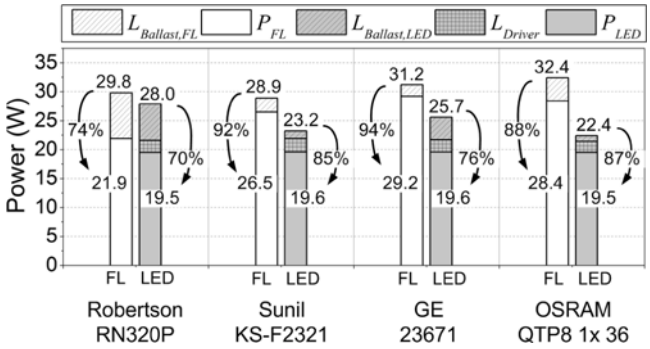

Fig. 20. Total power consumed from the ac supply, converter losses and load power with FL and LED lamp.

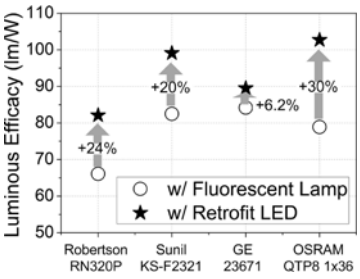

Fig. 21. Comparison of luminous efficacies using FL and retrofit LED lamp.

the FL, and were 0.99 and 8.7% with the LED lamp, respectively. Measured PF and THD of OSRAM QTP8 1×36 were 0.96 and 4.3% with the FL, and were 0.94 and 6.0% with the LED lamp, respectively.

D. Power Efficiency and Luminous Efficacy

In the retrofit LED system, both ballast and LED driver incur power losses. Power loss of the ballast $L_{\rm Ballast}$, power loss of the LED driver $L_{\rm Driver}$ and power consumed in the LED load $P_{\rm LED}$ are shown in Fig. 20. Lamp power and $L_{\rm Ballast}$ with the FL are provided together for comparison. The loss in the proposed LED driver $L_{\rm Driver}$ ranges from 1.9 to 2.3 W with different ballasts, and the efficiency of the driver alone is higher than 89.7%. However, as denoted in Fig. 20, the global efficiency from the ac supply is lower than that with the FL.

Nonetheless, it does not mean that the retrofit LED lamp is not useful. For the lighting devices, the luminous efficacy (lm/W) is usually compared instead of the power efficiency (W/W). The luminous efficacy of the T8 lamp is typically 90 lm/W and the efficiency of the ballast is multiplied to calculate the actual efficacy. Meanwhile, the lumen output of the 20-W LED load in this study is 2300 lm and it is divided by the input power from the ac supply to calculate the efficacy. Efficacies with both lamps are compared in Fig. 21. The luminous efficacy of the LED lamp is always higher than that of the FL. Furthermore, the light output of the LED lamp is directional and so called fixture efficiency is higher than that with the FL [30]. This is why the rated lumen output of the retrofit LED is only 2300 lm, whereas that of the FL is larger than 3000 lm. Therefore, even if the difference in luminous efficacy is only 6.2% in the worst case, the input power can be saved by 18% with the LED lamp. The improvements can be less with more efficient FLs, such as T5 lamps. It should be noted that the aforementioned discussions are based on assumed luminous fluxes, and lumen outputs need to be measured for a precise comparison.

The power loss in the LED driver is 2.1 W with the electronic ballast GE 23671, which exhibits the highest v_{C1} among the ballasts. Measured losses in rectifier and Schottky diode were 0.32 and 0.45 W, respectively. The controller (analog part) consumes 0.24 W. The switch is hard-switching and the total loss of the switch was measured to be 0.61 W. Finally, the remaining 0.51 W is conduction losses. The driver loss decreases slightly to 1.9 W with the electronic ballast OSRAM QTP8 1×36, which has the lowest v_{C1}. Soft-switching techniques may improve the driver efficiency by a few percent, but their applications are left as a further work.

VII. Conclusion

A ballast-compatible LED driver which adopts a CS boost converter has been proposed. A prototype 20-W LED driver is evaluated with T8 36-W FL ballasts. A startup process for emulating the high-voltage discharge enables the LED driver to operate normally with program-start ballasts. The LED driver successfully operates with both magnetic and electronic ballast, and achieves an accurate current regulation within 0.6% error. The luminous efficacy can be improved up to 30% with the LED lamp, even with the additional loss introduced by the ballast. The CS boost converter does not disturb the ballast operation so that certified features of the ballast, such as the power factor rating, are not degraded significantly.

Acknowledgment

The authors would like to thank engineers at HiDeep Inc., Gyeonggi-do, Korea for technical supports.

References

[1] International Energy Agency (IEA). (2013, Apr.). Energy prices and taxes—Quarterly statistics. Paris, France. [Online]. Available: http://dx.doi.org/10.1787/energy_tax-v2013-1-en

[2] R. D. Dupuis and M. R. Krames, "History, development, and applications of high-brightness visible light-emitting diodes," *J. Lightw. Technol.*, vol. 26, no. 9, pp. 1154–1171, May 2008.

[3] D. G. Lamar, M. Fernandez, M. Arias, M. M. Hernando, and J. Sebastian, "Tapped-inductor buck HB-LED AC–DC driver operating in boundary conduction mode for replacing incandescent bulb lamps," *IEEE Trans. Power Electron.*, vol. 27, no. 10, pp. 4329–4337, Oct. 2012.

[4] J. Zhang, H. Zeng, and T. Jiang, "A primary-side control scheme for high-power-factor led driver with triac dimming capability," *IEEE Trans. Power Electron.*, vol. 27, no. 11, pp. 4619–4629, Nov. 2012.

[5] R. Zhang and H. S.-H. Chung, "A TRIAC-dimmable LED lamp driver with wide dimming range," *IEEE Trans. Power Electron.*, vol. 29, no. 3, pp. 1434–1446, Mar. 2014.

[6] Y. Hu, L. Huber, and M. M. Jovanović, "Single-stage, universal-input ac/dc led driver with current-controlled variable PFC boost inductor," *IEEE Trans. Power Electron.*, vol. 27, no. 3, pp. 1579–1588, Mar. 2012.

[7] S. Wang, X. Ruan, K. Yao, S.-C. Tan, Y. Yang, and Z. Ye, "A flicker-free electrolytic capacitor-less AC–DC LED driver," *IEEE Trans. Power Electron.*, vol. 27, no. 11, pp. 4540–4548, Nov. 2012.

[8] M. Arias, M. F. Diaz, D. G. Lamar, D. Balocco, A. A. Diallo, and J. Sebastián, "High-efficiency asymmetrical half-bridge converter

without electrolytic capacitor for low-output-voltage AC–DC LED drivers," *IEEE Trans. Power Electron.*, vol. 28, no. 5, pp. 2539–2550, May. 2013.
[9] S. Moon, G.-B. Koo, and G.-W. Moon, "A new control method of interleaved single-stage flyback ac–dc converter for outdoor led lighting systems," *IEEE Trans. Power Electron.*, vol. 28, no. 8, pp. 4051–4062, Aug. 2013.
[10] F. Zhang, J. Ni, and Y. Yu, "High power factor ac–dc led driver with film capacitors," *IEEE Trans. Power Electron.*, vol. 28, no. 10, pp. 4831–4840, Oct. 2013.
[11] B. Lee, H. Kim, and C. Rim, "Robust passive LED driver compatible with conventional rapid-start ballast," *IEEE Trans. Power Electron.*, vol. 26, no. 12, pp. 3694–3706, Dec. 2011.
[12] N. Chen and H. S.-H. Chung, "An LED lamp driver compatible with low- and high-frequency sources," *IEEE Trans. Power Electron.*, vol. 28, no. 5, pp. 2551–2568, May 2013.
[13] (2014, Jan.). New InstantFit LED T8 from Philips Slashes Cost and time to replace Fluorescent Tubes with LED technology. [Online]. Available: http://www.newscenter.philips.com/us_en/standard/news/press/2014/20140108-instantfit-tled.wpd#.U7qMVfl_v-l
[14] (2014, May). Cree Delivers the First No-Compromise LED T8 Replacement Tube. [Online]. Available: http://www.cree.com/News-and-Events/Cree-News/Press-Releases/2014/May/T8-tube-release
[15] E. Deng and S. Ćuk, "Negative incremental impedance and stability of fluorescent lamps," in *Proc. IEEE Appl. Power Electron. Conf.*, 1997, pp. 1050–1056.
[16] R. J. Mckenzie, "Glow starter for electric discharge devices," U.S. Patent 2 426 463, Aug. 26, 1947.
[17] M. Rosiak, "Single lamp rapid start ballast," U.S. Patent 3 295 015, Dec. 27, 1966.
[18] J. C. W. Lam, S. Pan, and P. K. Jain, "A single-switch valley-fill power-factor-corrected electronic ballast for compact fluorescent lightings with improved lamp current crest factor," *IEEE Trans. Ind. Electron.*, vol. 61, no. 9, pp. 4654–4664, Sep. 2014.
[19] C. Ekkaravarodome, K. Jirasereeamornkul, and M. K. Kazimierczuk, "Implementation of a dc-side class-de low-dv/dt rectifier as a PFC for electronic ballast application," *IEEE Trans. Power Electron.*, vol. 29, no. 10, pp. 5486–5497, Oct. 2014.
[20] H. V. Marques, Á. R. Seidel, M. S. Perdigão, J. M. Alonso, and E. S. Saraiva, "Constant-frequency magnetically controlled universal ballast with sos compliance for tl5 fluorescent lamps," *IEEE Trans. Power Electron.*, vol. 27, no. 4, pp. 2163–2175, Apr. 2012.
[21] T.-H. Yu, L.-M. Wu, and T.-F. Wu, "Comparisons among self-excited parallel resonant, series resonant and current-fed push-pull electronic ballasts," in *Proc. IEEE Appl. Power Electron. Conf.*, 1994, pp. 421–426.
[22] M. K. Kazimierczuk and W. Szaraniec, "Electronic ballast for fluorescent lamps," *IEEE Trans. Power Electron.*, vol. 8, no. 4, pp. 386–395, Oct. 1993.
[23] E. Deng and S. Ćuk, "Single stage, high power factor, lamp ballast," in *Proc. IEEE Appl. Power Electron. Conf.*, 1994, pp. 441–449.
[24] R. W. Erickson and D. Maksimović, *Fundamentals of Power Electronics*, 2nd ed. New York, NY, USA: Springer, 2011.
[25] S. Ćuk, "General topological properties of switching structures," in *Proc. IEEE Power Electron. Spec. Conf. Rec.*, 1979, pp. 109–130.
[26] K.-H. Liu and F. C. Y. Lee, "Zero-voltage switching technique in DC/DC converters," *IEEE Trans. Power Electron.*, vol. 5, no. 3, pp. 293–304, Jul. 1990.
[27] J. Leppääho and T. Suntio, "Dynamic characteristics of current-fed super-buck converter," *IEEE Trans. Power Electron.*, vol. 26, no. 1, pp. 200–209, Jan. 2011.
[28] Standard for LED Equipment For Use in Lighting Products, Underwriters Laboratory, UL 8750, 2009.
[29] N. Chen and H. S.-H. Chung, "A driving technology for retrofit LED lamp for fluorescent lighting fixtures with electronic ballasts," *IEEE Trans. Power Electron.*, vol. 26, no. 2, pp. 588–601, Feb. 2011.
[30] "Energy efficiency and renewable energy, caliper report 21.4: Summary of linear (t8) led lamp testing," U.S. Department of Energy, Washington, DC, USA, Jun. 2014.

Jaeyoung Choi (S'08–M'14) received the B.S., M.S., and Ph.D. degrees in electrical engineering from the Korea Advanced Institute of Science and Technology, Daejeon, Korea, in 2007, 2009, and 2013, respectively.

In 2013, he joined the Institute of Microelectronics, Agency for Science, Technology, and Research (A∗STAR), Singapore, as a Research scientist, where he is currently involved in the development of CMOS RF/analog transceivers for wired and wireless communication systems. His research interests include CMOS RF/analog IC design for wireless communications and digitally controlled PMIC design.

Hee-Seok Han received the B.S., M.S., and Ph.D. degrees in electrical engineering from the Korea Advanced Institute of Science and Technology, Daejeon, Korea, in 2000, 2002, and 2007, respectively.

From 2007 to 2011 he worked as a R&D Engineer in Samsung Electronics, where he designed power management circuits for DDI & LED back-lighting applications. His research interests include design of switching converters and digitally controlled PMIC.

Kwyro Lee (M'80–SM'90–F'14) received the B.S. degree in electronics engineering from Seoul National University, Seoul, Korea, in 1976, and the M.S. and Ph.D. degrees in electrical engineering from University of Minnesota, Minneapolis, MN, USA, in 1983.

After graduation, he joined GoldStar Semiconductor Inc., Seoul, as an Engineering General Manager, responsible for development of the first poly-silicon CMOS products in Korea. Since 1986, he has been a Professor in the Department of Electrical Engineering at the Korea Advanced Institute of Science and Technology (KAIST), Daejeon, Korea. In 1997, he proposed and succeeded to host MICROS (Micro Information Communication Remote Object-oriented System) Research Center as a Director, which is supported by the Engineering Center of Excellence Program from Korea Science and Engineering Foundation. The MICROS is one of the world leading concepts of low power internet infrastructure currently known as Ubiquitous Sensor Network, or Internet of Things today. Between 1998 and 2000, and 2004 and 2005, he also served as the Dean of the KAIST Research Affairs. During 2005–2007, he was invited as an Executive Vice President of LG Electronics Inc. His responsibility was to direct LG Electronics Institute of Technology, which is the LG Electronics cooperate-wide central basic research center, consisted of Device and Material, Information, and Communication Technology Research Labs. In addition to the academic and industrial research, he also deeply involved in the public research policy as well. He served as a member of National Science and Engineering Council Organizing Committee directly reporting to the President of Korean government during 2008–2011. He served as the Chair of Leading Edge Convergence and Integration Technology Subcommittee as well. During 2010–2013, he worked as the President of the National Nano Fab Center, an independent organization affiliated with KAIST under the support of Ministry of Ministry of Science, ICT and Future Planning, and Daejeon City. He is one of the world pioneers on semiconductor device, RF CMOS circuit, and low-power wireless circuit design. He and his colleagues have published more than 150 papers in the international archival journals and more than 150 conference presentations. He holds 21 patents, and has written three books. He has also cofounded many fabless companies such as Integrant Technologies, Zinitix, Phychips, and Hi-Deep.

Dr. Lee is a member of the National Academy of Engineering of Korea.